Selective Cell Targeting with Light-Absorbing Microparticles and Nanoparticles

Costas M. Pitsillides,*† Edwin K. Joe,* Xunbin Wei,* R. Rox Anderson,* and Charles P. Lin*
*Wellman Laboratories of Photomedicine, Massachusetts General Hospital, Harvard Medical School, Boston, Massachusetts 02114 USA; and †Department of Mechanical Engineering, Massachusetts Institute of Technology, Cambridge, Massachusetts 02137 USA

ABSTRACT We describe a new method for selective cell targeting based on the use of light-absorbing microparticles and nanoparticles that are heated by short laser pulses to create highly localized cell damage. The method is closely related to chromophore-assisted laser inactivation and photodynamic therapy, but is driven solely by light absorption, without the need for photochemical intermediates (particularly singlet oxygen). The mechanism of light-particle interaction was investigated by nanosecond time-resolved microscopy and by thermal modeling. The extent of light-induced damage was investigated by cell lethality, by cell membrane permeability, and by protein inactivation. Strong particle size dependence was found for these interactions. A technique based on light to target endogenous particles is already being exploited to treat pigmented cells in dermatology and ophthalmology. With exogenous particles, phamacokinetics and biodistribution studies are needed before the method can be evaluated against photodynamic therapy for cancer treatment. However, particles are unique, unlike photosensitizers, in that they can remain stable and inert in cells for extended periods. Thus they may be particularly useful for prelabeling cells in engineered tissue before implantation. Subsequent irradiation with laser pulses will allow control of the implanted cells (inactivation or modulation) in a noninvasive manner.

INTRODUCTION

Intense efforts are being made in the use of monoclonal antibodies (mAbs) for targeting cytotoxic drugs and radionuclides to tumors and other diseased cells in the body. Despite much initial promise, the success of this line of therapy has so far been limited. Problems related to immunogenicity of the mAbs have been greatly reduced by the development of humanized antibodies (Dillman, 2001; White et al., 2000), but targeting specificity remains a key problem. One approach to reducing nonspecific tissue toxicity is the use of light-activated drugs that become toxic to cells only in areas that are exposed to light. This approach is attractive for tissue sites that are optically accessible—either by direct illumination or through fiber optic delivery. Photodynamic therapy (PDT) using immunoconjugated photosensitizers is an example of this treatment strategy (Del Governatore et al., 2000). However, PDT has its own set of challenges. One major problem is tissue oxygenation, since almost all current photosensitizers generate cytotoxicity through photochemical production of singlet oxygen as a reactive intermediate (Weishaupt et al., 1976; Fuchs and Thiele, 1998).

We describe a new method for selective cell targeting, based on the use of light-absorbing microparticles and nanoparticles conjugated to antibodies, which kills cells selectively upon exposure to short laser pulses. The method does not require photochemical generation of reactive intermediates. Instead, it is based on the creation of high peak temperatures and microscopic mechanical disruption that are localized at the cellular level when energy is selectively deposited into the particles. Selective energy deposition is accomplished by using laser pulses at a wavelength that is strongly absorbed by the particles but not by cells, and with a pulse duration that is sufficiently short to minimize heat flow away from the absorbing particles, a condition known as thermal confinement (Anderson and Parrish, 1983). Short laser pulses ensure that the absorbed energy does not have time to diffuse away from the particles during the laser pulse and is thus confined to the small volume of the absorber. The same principle is being used in human studies that employ short laser pulses to target pigmented cells containing endogenous melanin particles. In the eye for example, selective laser targeting of the retinal pigment epithelium is being investigated for the treatment of certain retinal disorders (Roider et al., 1992; Brinkmann et al., 2000), whereas selective laser trabeculoplasty (targeting pigmented trabecular meshwork cells) is in clinical trials for the treatment of open angle glaucoma (Latina and Tumbocon, 2002). In dermatology, laser removal of pigmented skin lesions is based on selective targeting of melanocytes (Anderson et al., 1989; Anderson, 2000).

To target specific cell populations that do not contain endogenous pigment particles, we use immunoconjugates of iron oxide microparticles or gold nanoparticles as light absorbers. Superparamagnetic iron oxide-doped latex microspheres are commercial products commonly used for magnetic cell separation, whereas immunogold nanoparticles are used extensively in electron microscopy due to their high electron density. Both types of particles strongly absorb visible light. Gold nanoparticles in particular have a distinct absorption peak near 520 nm that is size-dependent, as described by Mie (1908) in his theory of absorption and

Submitted June 14, 2002, and accepted for publication February 6, 2003.
Address reprint requests to Charles P. Lin, Wellman Laboratories of Photomedicine, Massachusetts General Hospital/Harvard Medical School, BHX 630, 40 Blossom St., Boston, MA 02114. Tel.: 001-617-724-3957; Fax: 001-617-724-2075; E-mail: lin@helix.mgh.harvard.edu.

0006-3495/03/06/4023/10 $2.00

scattering of light by small particles. To achieve thermal confinement, the pulse duration should be shorter than 1 μs for micrometer-sized particles, and shorter than 10 ns for particles smaller than 100 nm. In these studies, 20-ns laser pulses at 532 or 565 nm were used for both the micro- and nanoparticle experiments. Temperature calculations were performed to characterize the temperature distribution around the nanoparticle absorbers during the laser pulse. Nanosecond time-resolved microscopy was used to image transient cellular events in response to the laser exposure.

We have further exploited the ability of the nanoabsorbers to inflict localized damage to cells at sublethal levels, to transiently modify cellular functions without causing cell death. By adjusting particle numbers, size, and laser energy delivered to the targets it is possible to transiently increase the permeability of the plasma membrane, allowing the introduction of foreign molecules into living cells. A separate set of experiments was performed to investigate the possibility of using this technique to target specific protein molecules. Gold nanoparticles were bound to anti-fluorescein rabbit IgG antibody either directly or through a secondary antibody. The antibody-gold conjugate retains its ability to bind fluorescein and quench its emission upon binding. By measuring the degree of fluorescence quenching, we can determine the amount of protein that has been inactivated by short laser pulses. We show that this inactivation process is highly sensitive to the distance between the protein and the particle surface.

MATERIALS AND METHODS

Labeling of CD8+ lymphocytes with 0.83-μm iron oxide/latex spheres

The 0.83-μm streptavidin-coated, super paramagnetic iron oxide-doped latex spheres (Bangs Laboratories, Fisher, IN) were first suspended in PBS-BSA buffer (phosphate-buffered saline, 0.1% bovine serum albumin) and incubated with biotin-conjugated monoclonal anti-human CD8 mouse IgG (Sigma, St. Louis, MO) for 45 min at room temperature. The CD8 cell surface molecule is expressed on a subset of T lymphocytes (cytotoxic/supressor T cells), making it a good target for investigating selectivity in cell killing. To isolate the captured antibody, the microsphere suspension was placed in a magnetic separation rack for 3 min. The ligand-bound microspheres were added to a mixed population of human lymphocytes (isolated from whole blood of healthy human donors using Ficoll density gradient centrifugation) together with R-Phycoerythrin conjugated monoclonal anti-human CD8 mouse IgG (Sigma, St. Louis, MO) and incubated for 45 min at room temperature. Excess, unbound antibody was removed by suspending the cells in PBS-BSA buffer and centrifuging for 10 min at 300 $\times$ g (repeated three times). The cells were resuspended in buffer solution and placed in a LAB-TEK glass 2-well chamber slide for ~30 min at 37°C. The chamber slide was then flooded with cell culture medium (RPMI 1640, 10% fetal calf serum) and the cells were irradiated 30 min later. Cell viability was assayed using calcein-AM (Molecular Probes, Eugene, OR), at a concentration of 0.2 μg/ml, which was added to the suspension medium.

Labeling of CD8+ T lymphocytes with 30-nm gold spheres

Human lymphocytes isolated as described above from whole blood were incubated with unconjugated monoclonal anti-human CD8 mouse IgG and R-Phycoerythrin-conjugated monoclonal anti-human CD8 mouse IgG (both from Sigma, St. Louis, MO) for 30 min at room temperature. Excess, unbound antibody was removed by suspending in PBS-BSA buffer and centrifuging for 10 min at 300 $\times$ g (repeated three times). The cells were resuspended in buffer solution and placed in a LAB-TEK glass 2-well chamber slide for ~30 min at 37°C together with 30-nm gold particles conjugated to anti-mouse IgG (Nanoprobes, Stony Brook, NY). The chamber slide was then flooded with cell culture medium containing calcein-AM (0.2 μg/ml) and the cells were irradiated 30 min later.

Fluorescence microscopy and laser irradiation

Microparticle and nanoparticle-labeled lymphocytes were irradiated using a lab-developed imaging system employing stroboscopic illumination to detect transient cavitation at ~100 ns after the laser pulse. The strobe pulse was produced by using a beamsplitter to direct a small fraction of the irradiation beam through a time delay fiber imaged on the sample. The delay was variable but high-speed images were typically taken at 100 ns. Images were captured and digitized using a Cohu 4910 CCD (Cohu, Poway, CA) and a PC equipped with a frame-grabber board. Fluorescence images of the cells were taken before, immediately after and 1 h after irradiation. In both the microparticle and nanoparticle experiments, cells were irradiated with 20-ns, 565-nm pulses from a rhodamine dye cell pumped with the second harmonic output (532 nm) of a Q-switched Nd:YAG laser (Continuum, Santa Clara, CA). Calcein-AM fluorescence was excited at a wavelength of 488 nm by a cw Argon laser (Evergreen Laser Corporation, Durham, CT) whereas R-phycoerythrin (PE) was excited at 532 nm using a cw Nd:YAG (MWK Industries, Riverside, CA).

Labeling of CD45+ T lymphocytes with 30- and 20-nm gold spheres—membrane permeabilization

Human lymphocytes isolated from whole blood were suspended in PBS-BSA buffer (phosphate-buffered saline, 1% albumin) and incubated with monoclonal anti-human CD45 mouse IgG (Sigma, St. Louis, MO) for 30 min at room temperature. The antibody recognizes the CD45 antigen that is common to all leukocytes. The goal of this investigation was to determine efficiency, rather than selectivity, of cell membrane permeabilization. Therefore anti-CD45 antibody was chosen to label all leukocytes rather than a subpopulation of the cells. Excess, unbound antibody was removed by washing in buffer solution. The cells were then incubated with 30- or 20-nm gold particles conjugated to anti-mouse IgG (Nanoprobes, Stony Brook, NY and BBInternational, UK, respectively) for ~30 min at room temperature. After incubation, the cells were washed in buffer solution and transferred to a 2-well chamber slide. A quantity of 10-kDa fluorescein (FITC)-dextran conjugate (0.1 mM) (Molecular Probes, Eugene, OR) was added as a probe for membrane permeabilization, and the cell suspension was irradiated using a scanning irradiation setup. The scanning system employed 20-ns, 532-nm pulses from a Q-switched Nd:YAG laser (Continuum, Santa Clara, CA) and allowed the uniform irradiation of the 2-well chamber slides using a 2-mm laser beam spot. The cells were washed ~10 min after irradiation and the probe solution was replaced with RPMI 1640 culture medium containing propidium iodide (PI) (Sigma, St. Louis, MO), at a concentration of 5 μg/ml, to assay cell death. After a 10-min incubation with PI, the cells were washed in buffer solution and counted in a Becton-Dickinson FACS Calibur flow cytometer (Becton-Dickinson, Franklin Lakes, NJ).

To determine whether irradiating cells labeled with either 30- or 20-nm gold particles led to delayed cell death (apoptosis), separate experiments were carried out in which no FITC-dextran was present in solution during the laser scanning. At various time points (0, 2, 12, and 24 h) after irradiation, a standard apoptosis assay was performed by staining cells with FITC-Annexin V and propidium iodide (Molecular Probes, Eugene, OR), and quantifying fluorescence in a flow cytometer (Becton-Dickinson, Franklin Lakes, NJ).

Protein inactivation—conjugating target proteins to gold spheres

The target protein, anti-fluorescein rabbit IgG antibody (Sigma, St. Louis, MO), was coupled to 20-nm gold spheres by incubating with colloidal gold particles, either plain or conjugated to anti-rabbit IgG antibody (Nanoprobes, Stony Brook, NY), in a phosphate-buffered saline (PBS) solution. The protein-particle suspension was placed in a quartz cuvette and incubated with a known concentration of fluorescein (Sigma, St. Louis, MO). The cuvette was then placed in an ice bath and irradiated with 20-ns laser pulses at a wavelength of 532 nm using a Q-switched Nd:YAG laser (Continuum, Santa Clara, CA). Fluorescence of the solution was excited at a wavelength of 488 nm using a cw Argon laser (Evergreen Laser Corporation, CT) and quantified using an Oriel Instaspec IV CCD (Oriel Instruments, Stratford, CT) connected to a PC.

RESULTS

Microparticle targeting of lymphocytes

Peripheral blood lymphocytes were used to study cell killing by light-absorbing microparticles. Cells were incubated with 0.83-μm iron oxide-doped latex microspheres coated with anti-CD8 IgG, and double-labeled with anti-CD8 IgG conjugated to R-phycoerythrin which acted as a fluorescent marker of the CD8+ T lymphocytes. Under bright field microscopy, the microparticles were visible and were bound to the surface of a subset of the cell population (Fig. 1 *A*). These cells were identified as CD8+ by fluorescence microscopy when PE was excited (Fig. 1 *C*). Irradiating with short (20-ns) laser pulses at 565 nm led to rapid heating of the particles and vaporization of a thin layer of fluid surrounding each particle, producing a microscopic version of underwater explosion and cavitation bubble formation (Lin and Kelly, 1998; Lin et al., 1999). The bubbles were unstable, undergoing rapid expansion and collapse on the timescale of 0.1–1 μs, with a maximal expansion diameter of a few micrometers (depending on laser fluence). The short-lived microcavitation bubbles were visualized using time-resolved microscopy with stroboscopic illumination (Fig. 1 *B*). After laser irradiation, the fate of the cells was assessed by fluorescence microscopy, using calcein-AM (acetoxymethyl) as the cell viability probe. Calcein-AM is nonfluorescent, electrically neutral, and cell membrane-permeable. Once inside a cell, it is reduced by nonspecific esterases to calcein. Calcein is a derivative of fluorescein and exhibits fluorescence properties, with excitation/emission maxima at 490 and 520 nm respectively. The charged calcein molecules are retained by cells with intact plasma membranes. However, damage to cells that results in loss of membrane integrity leads to leakage of the dye and loss of fluorescence. Fluorescence images were taken before (Fig. 1 *D*) and 1 h after (Fig. 1 *E*) irradiation to determine leakage of calcein fluorescence indicating loss of cell viability. About 40 different fields containing ~40–50 lymphocytes each (from 4–5 independent experiments) were counted for the various exposure conditions and the results are summarized in Fig. 2. For single pulse exposure at 0.35 J/cm^2, 77% of the CD8+ cells lost viability, whereas only 2% of the CD8− cells were killed. For 20 pulses both specific and nonspecific cell killing increased slightly: 80% of the CD8+ and 6% of CD8− cell lost viability. The experiment was performed with an average particle to cell ratio of 5 that was found to be optimal. Higher particle to cell ratios resulted in more unbound particles in the solution and higher nonspecific killing. Lower particle to cell ratios resulted in less efficient targeting (data not shown).

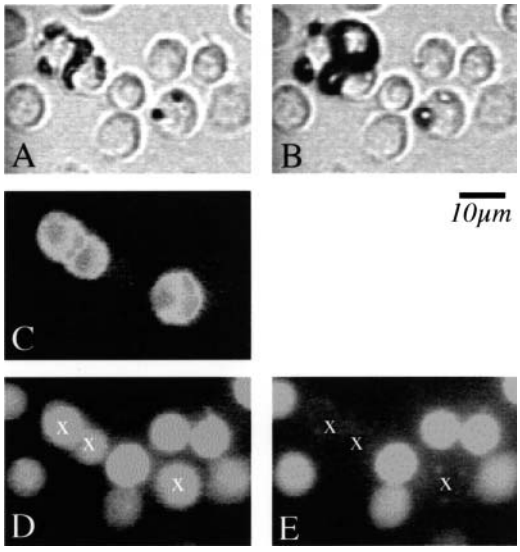

FIGURE 1 Lymphocytes labeled with anti-CD8 mAb-coated 0.83-μm iron oxide microspheres (5 particles/cell) and double-labeled with anti-CD8 phycoerythrin fluorescent probe. (*A*) is a bright field image. Iron oxide particles are visible on a subpopulation of the lymphocytes. (*B*) is a time-resolved image taken ~100 ns after irradiation with a 565-nm, 20-ns laser pulse at a fluence of 0.35 J/cm^2. Rapid growth of microbubbles can be seen around the particles. (*C*) is a fluorescence image which identifies CD8+ T cells (labeled with PE-conjugated anti-CD8 mAb). (*D*) and (*E*) are images of calcein-AM fluorescence before (*D*) and 1 h (*E*) after irradiation. Loss of fluorescence by CD8+ lymphocytes indicates loss of viability.

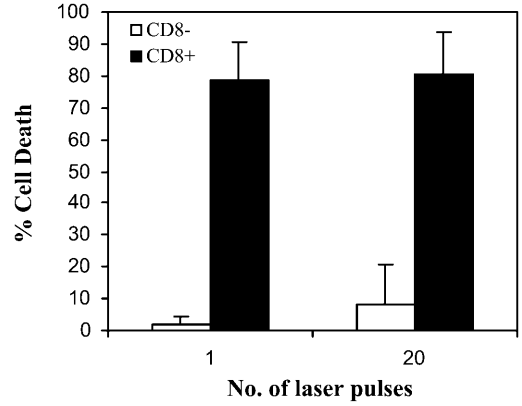

FIGURE 2 Viability of T lymphocytes labeled with anti-CD8 Ab + 0.83-μm iron oxide microspheres (5 particles/cell) after irradiation with 1 or 20 pulses (20-ns, 565-nm pulses at 0.35 J/ cm^2). Viability assayed 1 h after irradiation using calcein-AM fluorescence.

Nanoparticle targeting of lymphocytes

In the nanoparticle experiments, lymphocytes were first incubated with anti-CD8 mouse IgG and then with 30-nm gold particles conjugated to anti-mouse IgG antibody. Cells were double-labeled with anti-CD8-R-phycoerythrin probe to identify CD8+ T lymphocytes. The gold nanoparticles were not visible under a light microscope, and stroboscopic imaging during irradiation did not capture any transient cavitation events. Nonetheless, irradiating cells with 100 laser pulses (565-nm wavelength, 20-ns duration) at 0.5 J/cm^2 resulted in loss of viability, as determined by calcein-AM fluorescence assay. About 30 different fields containing ~50–60 CD8+/− cells each were counted for the various exposure conditions. Loss of calcein fluorescence in nonviable cells was often accompanied by changes in cell morphology such as cell swelling. Cell lethality for target cells increased from 54% with 100 Au particles/cell to 95% with 500 Au particles/cell. Lethality in untargeted cells (CD8−) varied from 5% to 8% over the same particle/cell range (Fig. 3).

Transient plasma membrane permealization using gold nanoparticles

To investigate transient cell membrane permeabilization using light-absorbing microparticles, 20-nm gold particles were attached to lymphocytes by incubating the cells first with anti-human CD45 mouse IgG antibody and then with gold particles conjugated to anti-mouse IgG antibody. The cells were irradiated with 20-ns, 532-nm laser pulses at a fluence of 0.5 J/cm^2 in the presence of 10-kDa fluorescein-dextran conjugate, a membrane-impermeable probe. After a 10-min incubation postirradiation, the probe was washed and the cells were double stained with propidium iodide to assay cell viability. The increase in uptake of the permeability probe (measured by the increase in mean FITC fluorescence) was analyzed for the viable cell population after excluding dead cells. The increase in probe uptake by viable cells was ~350% for 500 particles/cell and ~575% for the 2000 particle/cell ratio. Corresponding lethality also increased, and ranged from 14.5% to 40.2% of the total cell population (Fig. 4, *top*). To determine nonspecific uptake of the probe due to the presence of gold particles in the solution, control samples of cells were irradiated after incubation with the gold-antibody conjugates in the absence of primary anti-CD 45 antibody. To investigate the possibility that antibody/gold labeling of the cells might, by itself, increase the permeability of the plasma membrane, the uptake of the FITC-dextran probe was also quantified in samples of cells which were incubated with both antibodies, but which received no laser. Both control experiments showed no increase in fluorescence compared to untreated cells incubated

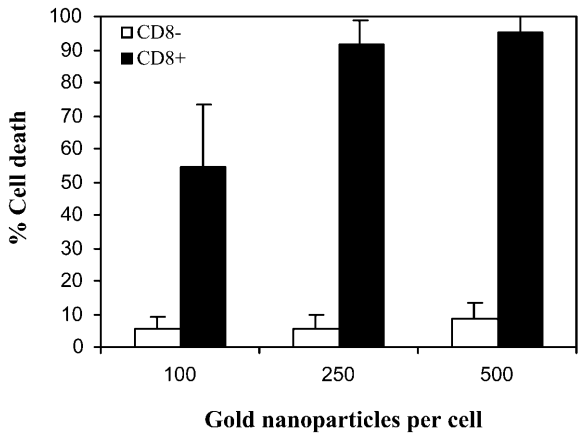

FIGURE 3 Viability of T lymphocytes labeled with 30-nm anti-CD8 immunogold particles, irradiated with 100 laser pulses (565 nm, 20 ns) at 0.5 J/cm^2. Calcein-AM fluorescence was used to assay viability 1 h after irradiation.

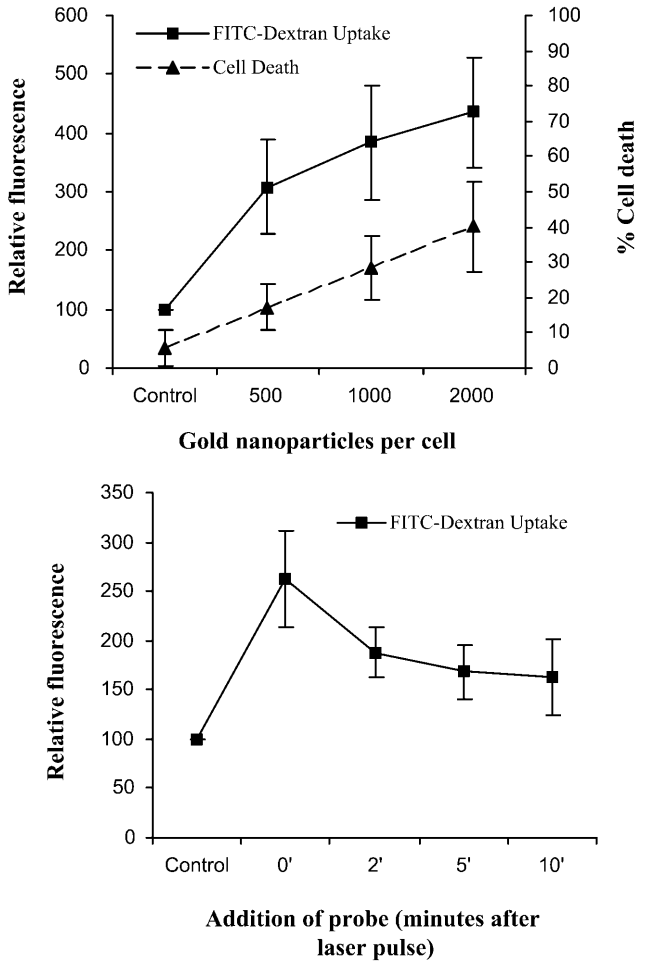

FIGURE 4 (*Top*) Increase in cell membrane permeability, assayed by FITC-dextran fluorescence uptake, of lymphocytes labeled with 20-nm anti-CD45 immunogold particles and irradiated with 20-ns laser pulses ($\lambda = 532$ nm) at 0.5 J/cm^2. (*bottom*) Adding the membrane permeability probe at different time points after irradiation indicates a rapid decline in probe uptake within 2 min.

with the FITC-dextran probe and indicated that transient plasma membrane permeabilization can only be achieved by irradiating cells in the presence of the gold nanoparticles when they are conjugated to the cell membrane.

To investigate the recovery time of the plasma membrane, the permeability probe was added to lymphocytes, labeled with 20-nm antibody-coated gold particles, at different time points after the application of the laser pulses. Fig. 4, *bottom*, shows the increase in probe uptake at 0, 2, 5, and 10 min after the laser. Nonlabeled cells were again irradiated in the presence of the probe to serve as controls. After the 2-min time point, the increase in probe uptake falls to the control level, suggesting that the plasma membrane recovers and reseals within 2 min after laser irradiation.

To investigate the possibility that membrane permeabilization is not a transient effect but may result in delayed cell death (apoptosis), experiments were carried out using annexin V/propidium iodide staining and flow cytometry to follow cell death up to 24 h postirradiation. Fig. 5 shows that almost all annexin V^+ cells are PI^+ (necrotic cells). There are very few PI^-annexin V^+ (apoptotic) cells. Moreover, there is very little change in necrotic cell fraction from 0 to

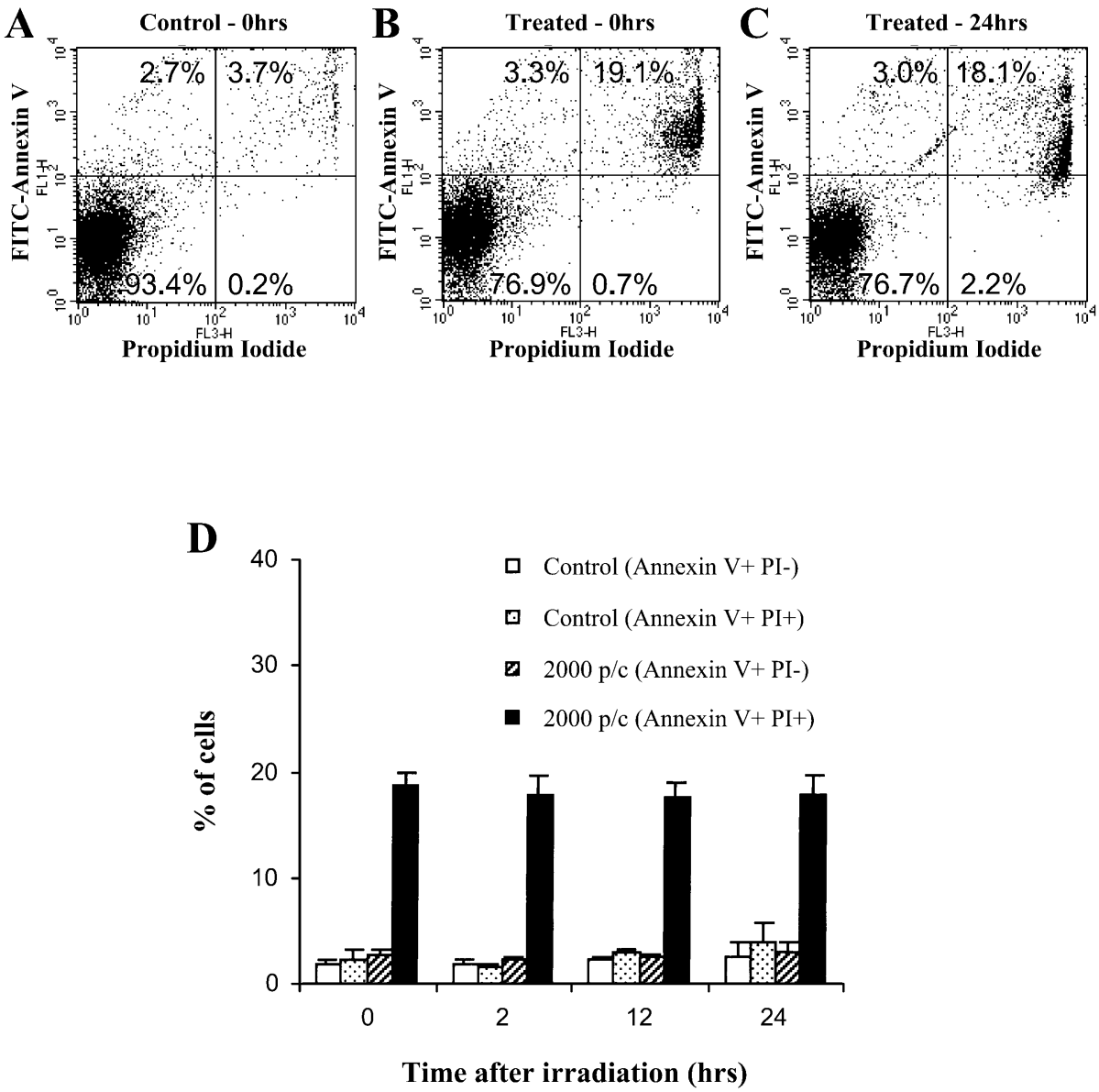

FIGURE 5 Cell death as a function of time after short pulse laser treatment of CD45+ lymphocytes labeled with 20-nm Au particles (2000 per cell) and irradiated with 20-ns laser pulses ($\lambda = 532$ nm) at 0.5 J/cm^2. Cells were analyzed by apoptosis/necrosis kit (annexin V/propidium iodide). Flow cytometry results (*A*) untreated cells, (*B*) immediately after irradiation, and (*C*) at 24 h after irradiation. The fraction of PI^+/Annexin V^+ cells (dead cell) remain constant during the 24-h period after irradiation (*D*). There was also no significant increase in the number of PI^-/Annexin V^+ cells (apoptotic cells) during this period.

24 h postirradiation, indicating that the fraction of cells that lost viability did so promptly. Conversely, the fraction of cells that were not killed immediately did not undergo apoptosis at a later time.

Protein inactivation using gold nanoparticles

Since the damage achieved using this technique is highly localized, we explored the possibility of employing the light-activated particles to target specific proteins in a functional knockout experiment. As a step toward that goal, we investigated the inactivation of a protein bound to gold nanopaticles. The protein chosen as the target was the anti-fluorescein rabbit IgG. The antibody binds to the molecules of the fluorescent dye fluorescein and quenches their laser-excited fluorescence (~3 antibody molecules per FITC molecule needed for complete quenching). This function can be used to design a simple assay to determine the antibody binding efficiency: active anti-FITC antibody quenches the laser-excited FITC fluorescence but the inactive antibody does not. Thus, measuring excited fluorescence in a solution containing the antibody and determining its quenching ability can yield information on the percentage of antibody that has been inactivated by laser irradiation.

By conjugating the anti-FITC antibody directly on the surface of the 20-nm Au particles and irradiating with 20-ns, 532-nm laser pulses at 0.2 J/cm^2, we were able to completely inactivate the protein. In a control experiment, the gold particles were coated with bovine serum albumin before incubating with the anti-FITC antibody. Irradiating the solution resulted in significantly less inactivation (~10%) as the antibody was now prevented from associating directly with the gold particles (Fig. 6).

To examine the distance effect of protein inactivation, the target antibody (primary mAb) was conjugated to the gold particles through a secondary mAb directed against anti-FITC IgG (indirect coupling). Irradiating the primary mAb/secondary mAb/gold particle conjugate resulted in decreased inactivation of the target as assayed by FITC fluorescence (Fig. 7). This result indicates that the extent of protein inactivation is dependent on distance from the gold particle. Inactivation of the primary mAb coupled to the secondary mAb/gold particle conjugate was only slightly higher than the control in which antibody was not associated with the gold during irradiation. An alternative explanation of this result is that we inactivated the secondary mAb that is attached to the gold surface, resulting in the dissociation of the primary from the secondary mAb. We did not determine whether the primary mAb remained bound to the secondary mAb after irradiation. However, even if this is the case, the primary mAb cannot diffuse away from the gold particle by any appreciable distance during the nanosecond heating cycle. We thus reach the same conclusion that protein molecules need to be directly bound to the gold particles to obtain efficient inactivation.

Temperature calculations

Temperature calculations were performed, based on a heat transfer model developed by Goldenberg and Tranter (1952) of a uniformly heated homogeneous sphere embedded in an infinite homogeneous medium, to characterize the temperature distribution in the gold nanoparticles and the surrounding fluid. For a sphere of radius R, generating heat for time $t > 0$ at a constant rate A per unit time per unit volume, the heat transfer equations are,

$$\frac{1}{k_1}\left(\frac{\partial}{\partial t}T_1\right) = \frac{1}{r^2}\left(\frac{\partial}{\partial r}\left[r^2\left\{\frac{\partial}{\partial r}T_1\right\}\right]\right) + \frac{A}{K_1}$$

$$\text{for } 0 \le r < R \quad \text{and} \quad t > 0$$

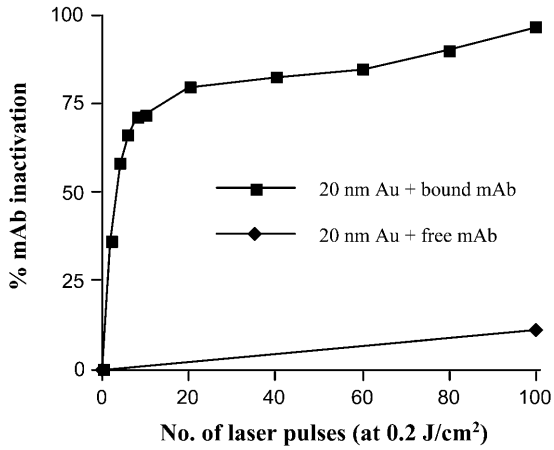

FIGURE 6 Inactivation of anti-fluorescein rabbit IgG conjugated to 20-nm gold particles. (■) represent results for inactivation of antibody when it is bound to the gold. (♦) are the results for antibody inactivation when the protein and gold are uncoupled.

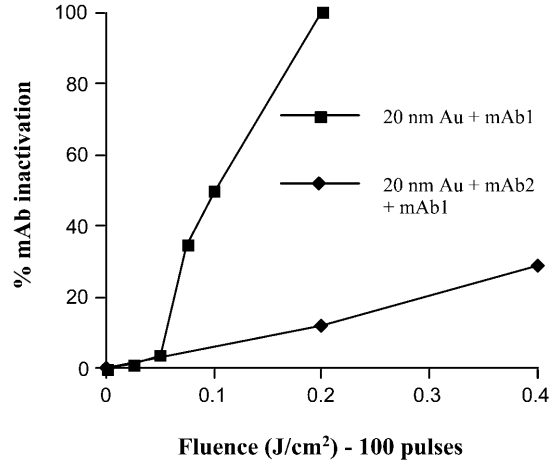

FIGURE 7 Inactivation of anti-fluorescein rabbit IgG—effect of distance of target from the gold particle absorber. (■) represent results for inactivation of the primary antibody (*mAb1*) when it is directly coupled to gold, whereas (♦) are the results for primary antibody inactivation when it is coupled to gold through a secondary antibody (*mAb2*).

$$\frac{1}{k_2}\left(\frac{\partial}{\partial t}T_2\right) = \frac{1}{r^2}\left(\frac{\partial}{\partial r}\left[r^2\left\{\frac{\partial}{\partial r}T_2\right\}\right]\right)$$
$$\text{for } r > R \quad \text{and} \quad t > 0.$$

The boundary conditions are, $T_1 = T_2$ at $t = 0$, $T_1 = T_2$ and $K_1((\partial/\partial r)T_1) = K_2((\partial/\partial r)T_2)$ at $r = R$, T_1 is finite as $r \to 0$ and T_2 is finite as $r \to \infty$ where T_1, T_2, K_1, K_2 and k_1, k_2 are the temperature, thermal conductivity, and diffusivity of the particle and the medium, respectively.

The solutions for the temperature distribution in and around the heated sphere are:

$$T_1 = \frac{R^2 A}{K_1}\left(\frac{K_1}{3K_2} + \frac{1 - \dfrac{r^2}{R^2}}{6} - \frac{2bR}{r\pi}\left[\int_0^{N\infty} \frac{\exp\left(\dfrac{-y^2 t}{a}\right)}{y^2} \frac{(\sin y - y\cos y)\sin\dfrac{ry}{R}}{(c\sin y - y\cos y)^2 + b^2 y^2 \sin^2 y}\,dy\right]\right)$$

and

$$T_2 = \frac{R^3 A}{rK_2}\left(\frac{K_1}{3K_2} - \frac{2}{\pi}\left[\int_0^{N\infty} \frac{\exp\left(\dfrac{-y^2 t}{a}\right)}{y^3} \frac{(\sin y - y\cos y)[by\sin y\cos wy - (c\sin y - y\cos y)\sin wy]}{(c\sin y - y\cos y)^2 + b^2 y^2 \sin^2 y}\,dy\right]\right),$$

where

$$a = \frac{R^2}{k_1}, \quad b = \frac{K_2}{K_1}\sqrt{\frac{k_1}{k_2}},$$
$$c = 1 - \frac{K_2}{K_1} \quad \text{and} \quad w = \left(\frac{R}{r} - 1\right)\sqrt{\frac{k_1}{k_2}}.$$

For the 30-nm Au particle, with an absorption coefficient, $Q_{abs} = 2$ at 532 nm and a laser fluence of 0.5 J/cm^2, the temperature rise is of the order of 2500 K at the end of the 20-ns pulse (Fig. 8). There was significant heat loss from the particle to the surrounding fluid, suggesting that even shorter pulses are necessary to achieve true thermal confinement. Nonetheless, the heated volume is highly localized to the vicinity of the particle with the 20-ns pulses. The temperature of the fluid falls to $1/e$ of the surface temperature at a distance of approximately one particle radius (15 nm).

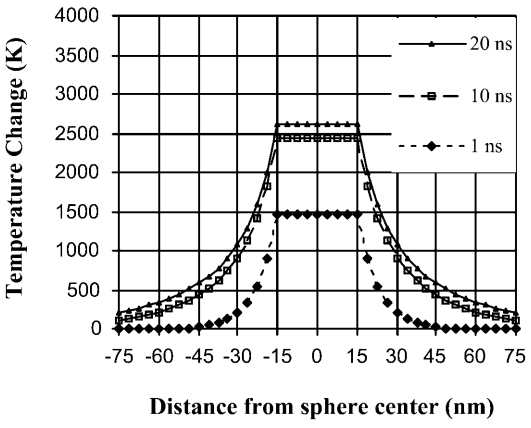

FIGURE 8 Theoretical temperature rise in a 30-nm gold particle ($Q_{abs} = 2$) irradiated with a 20-ns, 532-nm laser pulse at a fluence of 0.5 J/cm^2.

DISCUSSION

There has been a great deal of interest in recent years in the development of nanoparticle-based materials as biosensors (Kubitschko et al., 1997; Jones et al., 2001) and as drug carriers (Stella et al., 2000; Sershen et al., 2000). In comparison, very little attention has been paid to the use of nanoparticles for tissue and cell manipulation, i.e., as nanosurgery tools. Here we show that by binding particles to specific cell surface antigens and by localizing energy deposition into the particles, selective cell damage can be achieved without affecting neighboring cells. The laser fluence required for cell lethality (~0.5 J/cm^2) is moderate compared to the fluences currently used in clinical treatment of pigmented skin lesions (up to 5 J/cm^2).

Cellular microsurgery and nanosurgery have been performed in the past using tightly focused laser ''microbeams'' aimed at subcellular targets (Greulich and Pilarczyk, 1998; Konig et al., 1999). In the absence of a localized absorber, the interaction mechanism relies on nonlinear (multiphoton) absorption, and the size of the interaction zone is defined by the size of the laser focus, which is limited by diffraction to approximately $\lambda/2$, where λ is the optical wavelength. In contrast, in the current approach, the energy is absorbed by nanoparticles that can be much smaller than the wavelength of light. In addition, a large number of cells can be treated simultaneously using the micro/nanoparticle targeting approach without the need for precise aiming of the laser beam at individual cells.

The events that take place after the absorption of the laser pulse energy by small particles depend on the size of the absorber and the duration of laser exposure. Long pulses that exceed the thermal relaxation time of the target, t_r (where $t_r =$

$d^2/27k$ for uniform spheres of diameter d and thermal diffusivity k) cause heating of both the particle and the surrounding media as heat diffuses across the boundary. If the laser pulse duration is equal to or less than t_r then the energy can be thermally confined within the target, causing rapid heating of the absorber itself. The extreme temperature rise can induce explosive vaporization of a thin layer of fluid in contact with the particle, creating a vapor bubble that expands rapidly, on the nanosecond timescale (Lin et al., 1999), as the initial high vapor pressure overcomes the surface tension of the fluid. For micrometer-sized melanin particles, the temperature for bubble initiation has been estimated to be 140–150°C (Brinkmann et al., 2000), consistent with the degree of superheating necessary to overcome the surface tension associated with a nucleation size of 1 μm in water. As the bubble grows, the vapor cools and condenses. The bubble cannot sustain itself and implodes (Travena, 1978). The lifetime of the bubble is a function of its size at maximal expansion: for the microparticle absorbers, the bubble typically grows to a maximal size of a few micrometers (depending on laser fluence) and collapses on a timescale of 100 ns to 1 μs. A microscope with nanosecond time-resolution was required to visualize such short-lived microbubbles. A similar stroboscopic setup was previously used to study short-pulsed laser interaction with melanin microparticles in pigmented cells (Lin and Kelly, 1998).

Cavitation damage is the most like cause of cell death, because lethality is observed only when the laser fluence exceeds the threshold for cavitation bubble formation. In addition, the fluence needed for cell killing is about the same regardless of whether the particles are in the cytoplasm or on the cell surface, suggesting that, on such short time scales, thermal denaturation of proteins in the cell is not required for cell killing. Acoustic or shockwave damage is also not expected to play a major role because the pulse duration used in these studies is long compared to the stress relaxation time (acoustic transit time across the particles). The particles are not heated under inertial confinement (i.e., laser pulse is not short compared to the acoustic transit time of the absorber, so the particles were not heated under constant volume but were undergoing thermal expansion during the heating pulse), and therefore high pressure buildup is not expected at the particles. On the other hand, high pressures can arise during the final stage of bubble implosion and can contribute to damage caused by cavitation. It is interesting to note that the damage is highly localized, despite the underlying mechanism that can be regarded as a microscopic version of underwater explosion. Only those cells that have particles (internal or on the surface) are killed. Adjacent cells just a few micrometers away remain viable.

The mechanism underlying cell damage from gold nanoparticles is less clear. The 30-nm particles are not visible under light microscope, and attempts to image transient cavitation bubbles after laser irradiation were not successful. The smallest bubbles that we can visualize are produced around single 200-nm gold particles or around clusters of 30-nm particles when they are loaded at high concentrations into phagocytic cells (e.g., in endosomal/lysosomal compartments of macrophages). To gain some insights into the mechanism of interaction for individual 30-nm gold particles in the absence of direct visualization, numerical calculations were performed to estimate the temperature rise at the particles during the laser pulse. Using the model developed by Goldenberg and Tranter (1952), it can be shown that heat transfer is extremely rapid across the interface and that there is substantial heat loss from the gold particle into the surrounding medium during the 20-ns laser pulse. The thickness of the heated fluid layer is ~10–15 nm from the surface of the particle (Fig. 8). Despite the heat loss, the peak temperature at the particle exceeds 2000 K at a fluence of 0.5 J/cm^2 (the result of very strong plasmon resonance absorption of the gold). The high peak temperature exists only for nanoseconds, as the particle rapidly cools after the laser pulse. Electron micrographs of irradiated samples show fragmented gold particles (data not shown) consistent with a previous report by Kurita et al. (1998). In their paper, they report that they were able to fragment gold particles with mean diameters above ~14 nm, by irradiating colloidal gold solutions using Q-switched laser pulses at 532 nm. Particle fragmentation can result from direct laser heating of the gold to a temperature above its phase transition, or from the high pressure generated by the collapsing cavitation bubbles. Evidence for bubble formation around laser-heated colloidal gold particles was provided by studies using transient grating (four-wave mixing) spectroscopy (McEwan and Madden, 1992), where high-order nonlinear optical response associated with transient bubble formation was detected with 20- and 40-nm gold suspensions, but not with 5- and 10-nm suspensions. Irrespective of the exact mechanism, cells in our experiments were clearly damaged by the nanoexplosions that were too small to be detected by the optical imaging system.

Results from these studies show that particle size plays an important role in the cellular effect they create. With 0.83-μm particles, an average of 5 particles per cell results in 80% cell killing (Fig. 2), but increasing the particle/cell ratio beyond 5 led to an increase in both specific and nonspecific cell killing. In contrast, with 30-nm particles, increasing the particle/cell ratio to 500 resulted in greater lethality in targeted cells (95%), without substantial increase in nonspecific killing (Fig. 3). The reason is that the damage range of the nanoparticles was much smaller than the damage range of the microparticles. The nanoparticles had to be bound to cells to cause damage. Excess, unbound nanoparticles in solution did not cause appreciable damage. In contrast, excess microparticles settle down with the cells and cause nonspecific damage. A surprisingly large difference was also found between 20- and 30-nm particles. We were able to achieve membrane permeabilization with 20-nm particles without killing cells, whereas with 30-nm particles most of the cells were either killed (above threshold) or there was no

effect (below threshold). This strong particle size dependence was also obtained in the four-wave mixing studies (McEwan and Madden, 1992) and the particle fragmentation studies (Kurita et al., 1998) cited above. In particular, Kurita and coworkers found that irradiation of particles >20 nm led to significant reduction of particle size, whereas irradiation of particles <20 nm results in little change. Although we were not able to image cavitation with either 20- or 30-nm particles, it is possible that cell killing requires cavitation or particle fragmentation (both can be considered forms of underwater nanoexplosions). The smaller particles may fail to ''explode'' because they require a higher threshold for cavitation (a growing bubble needs to overcome surface tension that is inversely proportional to the particle size) (Huettmann and Birngruber, 1999). The observations of strong particle size effect in the 10–40-nm size range, using experimental techniques as diverse as four-wave mixing, particle sizing, and cell killing, may be different manifestations of the same physical phenomenon.

The ability to inflict lethality with ~500 nanoparticles per cell provides a useful contrast with immunotargeted PDT, which requires on the order of 10^6 molecules per cell (Vrouenraets et al., 2001). Therefore antibody-conjugated particles may be more efficient than PDT against cells that do not express high level of epitopes. Additional advantages of using light-particle interaction over the photochemical approach are a), the thermomechanical interaction is independent of oxygen, and b), the possibility of using near infrared light (>800 nm) that has better tissue penetration. Near-infrared light cannot drive photochemical processes, but nanoparticles with long wavelength absorption bands are now available by engineering their size, shapes, and composition (West and Halas, 2000). However, phamacokinetics and biodistribution studies are needed before the method can be evaluated against PDT for cancer treatment.

The ability to cause transient increase in the cell membrane permeability opens up the possibility to introduce foreign molecules (such as drugs, genes, or proteins) into selective living cells under light control. Selectively inactivating protein molecules bound to the surface of the nanoparticle absorbers offers the prospect of targeting specific cellular components (e.g., to inactivate a plasma membrane receptor) rather than whole cells, a potentially useful tool for basic cell biology research as well as to achieve a therapeutic effect. Single protein inactivation by laser excitation of antibody-coupled chromophores has already been applied to target single proteins on living cells (Jay and Sakurai, 1999; Beck et al., 2002) with promising results in identifying targets for cancer therapy.

We thank Dr. Mehran Poureshagh, Gereon Huettman, and Beno Radt for their valuable comments and assistance.

The study was supported by the US Department of Defense Medical Free Electron Laser Program under Grant No. F4 9620-01-1-0014 and by the Milton Fund of Harvard University. CMP was supported, in part, by the Alexander Onassis Public Benefit Foundation.

REFERENCES

Anderson, R. R. 2000. Lasers in dermatology—a critical update. *J. Dermatol.* 27:700–705.

Anderson, R. R., R. J. Margolis, S. Watenabe, T. Flotte, G. J. Hruza, and J. S. Dover. 1989. Selective photothermolysis of cutaneous pigmentation by Q-switched Nd:YAG laser pulses at 1064, 532, and 355 nm. *J. Invest. Dermatol.* 93:28–32.

Anderson, R. R., and J. A. Parrish. 1983. Selective photothermolysis: precise microsurgery by selective absorption of pulsed radiation. *Science.* 220:524–527.

Beck, S., T. Sakurai, B. K. Eustace, G. Beste, R. Schier, F. Rudert, and D. G. Jay. 2002. Fluorophore-assisted light inactivation: a high throughput tool for direct target validation of proteins. *Proteomics.* 2:247–255.

Brinkmann, R., G. Huettmann, J. Roegener, J. Roider, R. Birngruber, and C. P. Lin. 2000. Origin of retinal pigment epithelium cell damage by pulsed laser irradiance in the nanosecond to microsecond time regimen. *Lasers Surg. Med.* 27:451–464.

Del Governatore, M., M. R. Hamblin, C. R. Shea, I. Rizvi, K. G. Molpus, K. K. Tanabe, and T. Hasan. 2000. Experimental photoimmunotherapy of hepatic metastases of colorectal cancer with a 17.1A chlorin(e6) immunoconjugate. *Cancer Res.* 60:4200–4205.

Dillman, R. O. 2001. Monoclonal antibodies in the treatment of malignancy: basic concepts and recent developments. *Cancer Invest.* 19:833–841.

Fuchs, J., and J. Thiele. 1998. The role of oxygen in cutaneous photodynamic therapy. *Free Radic. Biol. Med.* 24:835–847.

Goldenberg, H., and C. J. Tranter. 1952. Heat flow in an infinite medium heated by a sphere. *Brit. J. Appl. Phys.* 3:296–298.

Greulich, K. O., and G. Pilarczyk. 1998. Laser tweezers and optical microsurgery in cellular and molecular biology. Working principles and selected applications. *Cell. Mol. Biol.* 44:701–710.

Huettmann, G., and R. Birngruber. 1999. On the possibility of high-precision photothermal microeffects and the measurement of fast thermal denaturation of proteins. *IEEE J. Quant. Electr.* 5:954–962.

Jay, D. G., and T. Sakurai. 1999. Chromophore-assisted laser inactivation (CALI) to elucidate cellular mechanisms of cancer. *Biochim. Biophys. Acta.* 1424:M39–M48.

Jones, R. M., L. Lu, R. Helgeson, T. S. Bergstedt, D. W. McBranch, and D. G. Whitten. 2001. Building highly sensitive dye assemblies for biosensing from molecular building blocks. *Proc. Natl. Acad. Sci. USA.* 98:14769–14772.

Konig, K., I. Riemann, P. Fischer, and K. J. Halbhuber. 1999. Intracellular nanosurgery with near infrared femtosecond laser pulses. *Cell. Mol. Biol.* 45:195–201.

Kubitschko, S., J. Spinke, T. Bruckner, S. Pohl, and N. Oranth. 1997. Sensitivity enhancement of optical immunosensors with nanoparticles. *Anal. Biochem.* 253:112–122.

Kurita, H., A. Takami, and S. Koda. 1998. Size reduction of gold particles in aqueous solution by pulsed laser irradiation. *Appl. Phys. Lett.* 72:789–791.

Latina, M. A., and J. A. Tumbocon. 2002. Selective laser trabeculoplasty: a new treatment option for open angle glaucoma. *Curr. Opin. Ophthalmol.* 13:94–96.

Lin, C. P., and M. W. Kelly. 1998. Cavitation and acoustic emission around laser-heated microparticles. *Appl. Phys. Lett.* 72:2800–2802.

Lin, C. P., M. W. Kelly, S. A. B. Sibayan, M. A. Latina, and R. R. Anderson. 1999. Selective cell killing by microparticle absorption of pulsed laser radiation. *IEEE J. Quant. Electr.* 5:963–968.

McEwan, K. J., and P. A. Madden. 1992. Transient grating effects in absorbing colloidal suspensions. *J. Chem. Phys.* 97:8748–8759.

Mie, G. 1908. Beitrage zur Optik truber Medien speziell kolloidaler Metallosungen. *Ann. Phys.* 25:377–445.

Roider, J., N. A. Michaud, T. J. Flotte, and R. Birngruber. 1992. Response of the retinal pigment epithelium to selective photocoagulation. *Arch. Opthalmol.* 110:1786–1792.

Sershen, S. R., S. L. Westcott, N. J. Halas, and J. L. West. 2000. Temperature-sensitive polymer-nanoshell composites for photothermally modulated drug delivery. *J. Biomed. Mater. Res.* 51:293–298.

Stella, B., S. Arpicco, M. T. Peracchia, D. Desmaele, J. Hoebeke, M. Renoir, J. D'Angelo, L. Cattel, and P. Couvreur. 2000. Design of folic acid-conjugated nanoparticles for drug targeting. *J. Pharm. Sci.* 89:1452–1464.

Travena, D. H. 1978. Cavitation and Tension in Liquids. IOP, Bristol, UK.

Vrouenraets, M. B., G. W. M. Visser, M. Stigter, H. Oppelaar, G. B. Snow, and G. A. M. S. van Dongen. 2001. Targeting of aluminum (III) phthalocyanine tetrasulfonate by use of internalizing monoclonal antibodies: improved efficacy in photodynamic therapy. *Cancer Res.* 61:1970–1975.

Weishaupt, K. R., C. J. Gomer, and T. J. Dougherty. 1976. Identification of singlet oxygen as the cytotoxic agent in photoinactivation of a murine tumor. *Cancer Res.* 36:2326–2329.

West, J. L., and N. J. Halas. 2000. Applications of nanotechnology to biotechnology. *Curr. Opin. Biotechnol.* 11:215–217.

White, C. A., R. L. Weaver, and A. J. Grillo-Lopez. 2000. Antibody-targeted immunotherapy for treatment of malignancy. *Annu. Rev. Med.* 52:125–145.